Letter | Editors' Suggestion

Interplay between many-body correlations, strain, and lattice relaxation in twisted bilayer graphene

Lorenzo Crippa,[1,*] Gautam Rai,[1,2,*] Dumitru Călugăru,[3,4] Haoyu Hu,[5] Jonah Herzog-Arbeitman,[3] B. Andrei Bernevig,[3,5,6] Roser Valentí,[7] Giorgio Sangiovanni,[8] and Tim Wehling[1,2]

[1]*I. Institute of Theoretical Physics, University of Hamburg, Notkestrasse 9, 22607 Hamburg, Germany*

[2]*The Hamburg Centre for Ultrafast Imaging, 22761 Hamburg, Germany*

[3]*Department of Physics, Princeton University, Princeton, New Jersey 08544, USA*

[4]*Rudolf Peierls Centre for Theoretical Physics, University of Oxford, Oxford OX1 3PU, United Kingdom*

[5]*Donostia International Physics Center, P. Manuel de Lardizabal 4, 20018 Donostia-San Sebastian, Spain*

[6]*IKERBASQUE, Basque Foundation for Science, Bilbao, Spain*

[7]*Institut für Theoretische Physik, Goethe Universität Frankfurt, Max-von-Laue-Strasse 1, 60438 Frankfurt am Main, Germany*

[8]*Institut für Theoretische Physik und Astrophysik and Würzburg-Dresden Cluster of Excellence ctd.qmat, Universität Würzburg, 97074 Würzburg, Germany*

(Received 14 October 2025; revised 29 May 2026; accepted 2 June 2026; published 17 June 2026)

In twisted bilayer graphene, a unified understanding of the mechanisms governing temperature-dependent electronic spectra and thermodynamic properties remains controversial despite extensive theoretical efforts. Here, we present a comprehensive theoretical framework that quantitatively accounts for scanning tunneling spectroscopy, quantum twisting microscopy, and thermodynamic properties of magic angle twisted bilayer graphene. We demonstrate that the observed behavior arises from the interplay between electron correlations and external symmetry breaking induced by strain and lattice relaxation. These effects act cooperatively to shape the emergent electronic behavior, leaving characteristic signatures across spectroscopy, compressibility, and entropy.

DOI: 10.1103/x2mz-hm8y

Introduction. Strain and lattice relaxation are ubiquitous effects in graphene moiré systems such as twisted bilayer graphene (TBLG). Strain asymmetrically stretches the hexagonal moiré unit cell of the system, as sketched in Fig. 1(a). TBLG samples typically have substantial heterostrain ($\epsilon = 0.1\%$–0.4%), stemming from several sources during sample preparation and handling, with ultralow-strain samples ($\epsilon < 0.1\%$) being rare [1–4]. Typical and ultralow-strain samples are known to feature different correlated insulating states at low temperatures [1], highlighting the need for the modeling of electron correlations in the presence of lattice effects [3–10].

Lattice relaxation follows from the energetics of the emergent moiré pattern, as local AB (Bernal) regions are energetically favored compared to the local AA (aligned) regions. This results in both in-plane and out-of-plane deformations of the atomistic graphene structure, causing the AA regions to shrink relative to the AB regions and bringing the two layers closer to each other at the AB regions compared to the AA regions [6,10–13].

Both strain and lattice relaxation effects reduce the symmetries of the system. In the absence of perturbations, TBLG is well described by the seminal Bistritzer-MacDonald (BM) continuum model [[14] and Fig. 1(b)] which, in addition to the translational symmetries and $SU(2)$ spin symmetry, possesses $C_{3z}, C_{2x}, C_{2z}, \mathcal{T}$ symmetries and an emergent anticommuting particle-hole symmetry P. Heterostrain generically breaks C_{3z} and C_{2x}, splitting the flat band manifold, while lattice relaxation breaks P [15], causing the upper flat bands to become more dispersive than the lower flat bands.

In this paper we show that the breaking of some of the lattice and particle-hole symmetries, together with a proper evaluation of electronic correlations, are the key to unlocking a unified description of three ubiquitous and hitherto unexplained features observed in TBLG experiments: (i) the emergence of a filling-independent persistent spectral feature at $V_b \sim 10$ meV in the local spectral function [5,9,16]; (ii) a transition from eightfold degenerate to fourfold degenerate local moments in the flat band manifold when lowering the temperature [5,17,18]; and (iii) the particle-hole asymmetry of positive vs negative fillings measured from the charge neutrality point (CNP), with charge compressibility varying more strongly on the electron (e)-doped side [9,17–20], and superconductivity showing higher stability on the hole (h)-doped side [21–23] across many samples.

We find that typical strain values $\sim 0.1\%$ induce a crystal-field-like splitting of the flat-band manifold of the order of 10 meV. This directly results in a ~ 10 meV persistent feature in the local density, that matches the filling-independent peak reported in [9,16].

Furthermore, our results show that relaxation-induced particle-hole asymmetry in the noninteracting dispersion

[*]These authors contributed equally to this work.

Published by the American Physical Society under the terms of the Creative Commons Attribution 4.0 International license. Further distribution of this work must maintain attribution to the author(s) and the published article's title, journal citation, and DOI.

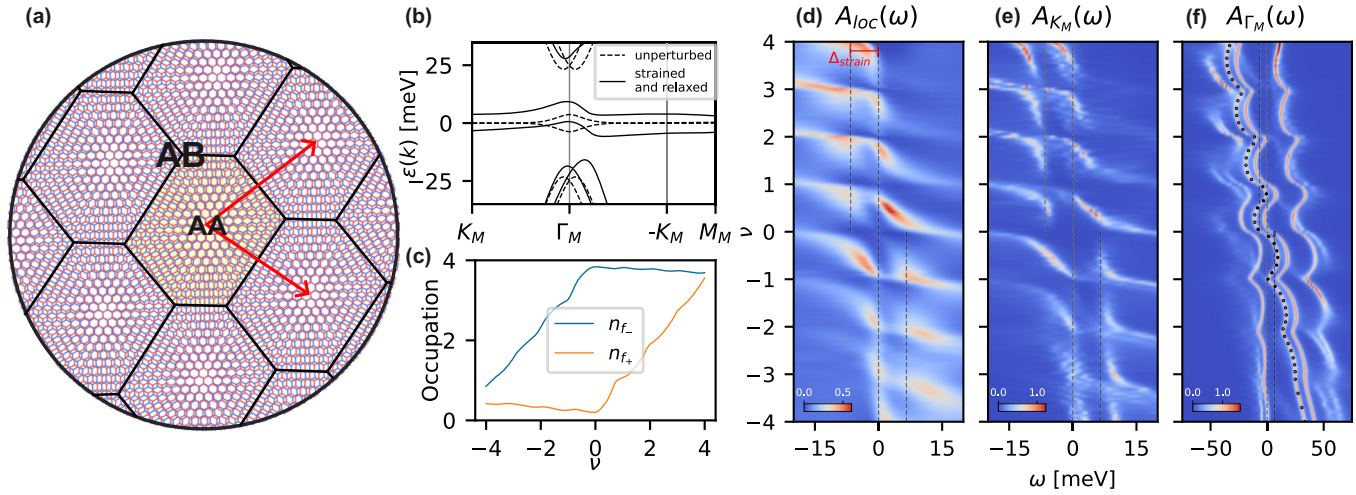


FIG. 1. (a) Sketch of strained twisted bilayer graphene lattice structure. The red arrows represent the moiré lattice vectors, while the shaded area is the strained unit cell. (b) Noninteracting dispersion of the unperturbed (dashed) and strained and relaxed (solid) THF models for the K valley. (c) Occupation of the f_+ and f_- orbitals as a function of filling. (d) Local (mBZ averaged) spectral function. (e) Spectral function at the K_M point and (f) at the Γ_M point for fillings $\nu \in [-4, 4]$ with 0.15% uniaxial heterostrain and lattice relaxation. All data are in the symmetric phase and for $T = 11.6$ K. The black dotted line in (f) is the $\mu(\nu)$ curve. The dashed vertical lines are drawn at $\pm M_f \epsilon_-$ which is the magnitude of the strain-induced splitting in the noninteracting model.

carries over to the interacting system physics, with stronger variations in the charge compressibility on the electron-doped side compared to the hole-doped side.

Interestingly, we find that in typically strained samples, when the system is doped away from the charge neutrality point, correlations are largely frozen in the inactive (away from the Fermi level) flat-band sector, and present in the active (crossing the Fermi level) flat-band sector. This has strong implications for the degeneracy of the local moments, as is observed in the entropy as a function of filling, which progressively vanishes at the CNP as the temperature is lowered below the characteristic scale of the strain splitting, in good agreement with recent experimental data [5].

Model and methods. In order to correctly describe the dynamical properties of the (magic angle) MA-TBLG electronic structure, we make use of the topological heavy fermion model (THF) [24], which represents the physics of the flat bands in terms of maximally localized Wannier orbitals accurately mapping the BM continuum model for 1.05°-twisted bilayer graphene to a generalized periodic Anderson model [24]. Per moiré unit cell, two localized f orbitals (per spin and valley) represent the maximally localized Wannier functions, which are centered in the AA-stacked regions, transform like $p_x \pm ip_y$ orbitals under the symmetries of TBLG, and capture ∼96% of the flat band spectral weight. Four dispersive c orbitals (per spin and valley) make up most of the two closest remote bands above and below the flat-band manifold and guarantee the correct elementary band representation of the flat bands by virtue of mode hybridization at the Γ_M point. Per spin and valley, the noninteracting Hamiltonian can be written in the form of a 6×6 matrix $H^{\eta}_{\mathrm{HF}}(k)$ acting on the spinor $(f^{\eta}_{\alpha}, c^{\eta}_{a})$ with $a = 1, 2, 3, 4$ and $\alpha = 1, 2$ representing the orbitals and $\eta = K, K'$ representing the valleys.

The THF model can be naturally extended [15,25] to describe strain and lattice relaxation effects [26,27] which are described by local single particle terms. Reference [15] shows that the modifications to the band structure due to strain and lattice relaxation can be incorporated—directly from *ab initio* continuum studies [26–28]—into the THF model via first-order perturbation theory, resulting in the perturbed Hamiltonian $H^{\eta}_{\mathrm{HF},\epsilon,\Lambda}$,

$$H^{\eta}_{\mathrm{THF},\epsilon,\Lambda}(\mathbf{k}) = H^{\eta}_{\mathrm{THF}}(\mathbf{k}) + \delta H^{\eta}_{\epsilon} + \delta H^{\eta}_{\Lambda}(\mathbf{k}), \tag{1}$$

where $\delta H^{\eta}_{\epsilon}$, $\delta H^{\eta}_{\Lambda}(\mathbf{k})$ represent the corrections due to strain and relaxation, respectively, ϵ parametrizes the uniaxial heterostrain, and Λ parametrizes the nonlocal tunneling terms stemming from lattice relaxation.

The primary effect of $\delta H^{\eta}_{\Lambda}$ is the introduction of two orbital-dependent chemical potential terms that shift the two pairs of c electrons relative to each other and to the f electrons, thus breaking P symmetry. The strain term $\delta H^{\eta}_{\epsilon}$, instead, incites f-orbital hybridization causing the flat-band manifold to split. At 0.15% strain, an average value of the typical strain magnitude found in most samples, the split is about 7 meV. Figure 1(b) shows the typical band structure with strain and lattice relaxation included. In the following, we will refer to the split narrow bands as the bonding and antibonding flat bands, and to the local eigenfunctions of the strained f-subspace Hamiltonian (which are eigenstates of σ_y) as the f_- and f_+ orbitals.

To model Coulomb interaction in this setup, we assume a double-gate screened interaction with an intergate distance $\xi = 10$ nm and dielectric constant $\epsilon = 6$. From this, we deduce the value of the many-body interaction coefficients, with the dominant term being the ff-interaction $U = 57.95$ meV, and the cf and cc terms circa 15 meV weaker. Given the width of the narrow bands is of the order of 10 meV [15,24,25], the interaction-to-bandwidth ratio implies that correlation effects are extremely pronounced. In fact, theoretical simulations show how a mean-field description is not very accurate in capturing spectral and response properties of the system, as well

as the temperature scale for phase transitions [29,30]. Hence, we employ the charge self-consistent dynamical mean-field theory (DMFT) framework developed in [29,31], making use of the CT-QMC solver *w2dynamics* [32] to study the effects of correlations in the presence of strain and lattice relaxation in absence of spontaneous symmetry breaking. We treat the f-subspace local interactions at all orders, and all other nonlocal two-body terms, which fall outside the DMFT approximation, at the Hartree level by coupling to the self-consistently adjusted density matrix. We disregard spontaneous symmetry breaking by setting a temperature of $T \geqslant 11.6\,\mathrm{K}$, above the onset of ordering [29]. For more details on the solver and method see [25].

Spectral persistent feature and charge sector freezing. In Figs. 1(d)–1(f) we show how the spectral function of TBLG evolves with filling when both strain and lattice relaxation are included. The results presented here refer to a strain level 0.15%. The dependence of the spectra on the strain mangitude is discussed in the end matter. These figures can be compared directly with the local density measured via scanning tunneling microscopy (STM) [7,9,10,33,34] and the Quantum twisting microscope [16,35,36], as well as the previous DMFT data on unstrained models [29,30]. Similarly to the unstrained and unrelaxed system, the spectral function features cascade transitions, with side bands forming patterns that repeat every time the number of electrons per moiré unit cell changes by an integer, and the f- and c-electron occupations resetting. However, the spectra from the perturbed model reproduce one important feature in the experimental data that has thus far eluded explanation. QTM [16] and STM [9] spectra report the presence of a "persistent" (filling-independent) feature at around $\sim$10 meV on the h-doped site and $\sim -10\,\mathrm{meV}$ on the e-doped side. While this feature was absent in previous unstrained DMFT calculations [29,30], our spectral functions of the perturbed model reproduce the persistent feature [cf. the dashed vertical lines in Figs. 1(d)–1(f)] and provide a natural explanation for the corresponding excitations.

Figure 1(d) shows the local spectral function (i.e., averaged over the mini BZ of TBLG), while (e) and (f) are the spectral functions at the K_M and Γ_M high-symmetry points. The theoretical data are in good agreement with the QTM results at the corresponding momenta [16]. At the K_M point, the spectrum presents a well defined gap around the Fermi energy, which is maximum around the CNP. The local spectral function, however, features residual spectral resonance crossing the gap. This is mostly due to the c-electron spectral weight at Γ_M, as explained in detail in [25]. Since the c electrons are weakly correlated, the associated spectral peaks effectively behave as noninteracting bands, rigidly shifting upon chemical potential variations. This gives rise to the striking correspondence between the central spectral peak and the $-\mu(\nu)$ curve, represented by the black dotted line in Fig. 1(f), which is also observed experimentally in [16].

The breaking of C_{3z} by strain causes the eightfold degenerate flat-band manifold in the unperturbed THF to split into two sets of degenerate antibonding and bonding f bands. In Fig. 1(c), we follow the occupation of the f_+ and f_- electrons as a function of total filling ν. We find that on the e-doped side, the f_- manifold occupation is almost complete and constant, while the f_+ electrons are active, and vice versa on the h-doped side. This suggests that the persistent feature is related to excitations to the inactive sector. Since this switches at the charge neutrality point, it appears at positive or negative bias depending on whether the system is hole or electron doped, and the energy at which it appears depends on the magnitude of strain in the sample.

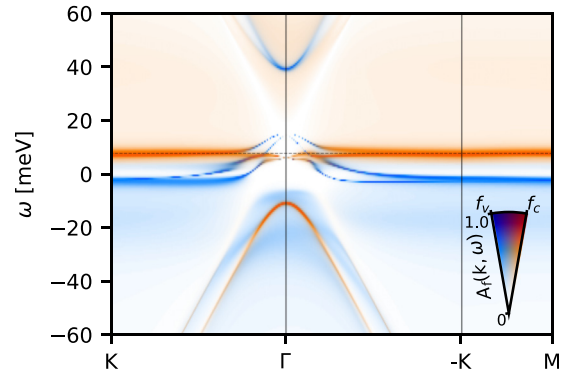


FIG. 2. Momentum-resolved f-projected spectral function with lattice relaxation and 0.15% strain at filling $\nu = -0.8$ and $T = 11.6\,\mathrm{K}$, projected onto the strain split f_+ (orange) and f_- (blue) orbitals. On the h-doped side ($\nu < 0$), the persistent feature at around 10 meV is made up of unoccupied f_+ spectral weight.

We confirm this hypothesis by looking at the momentum-resolved spectral function in Fig. 2, obtained at $T = 11.6\,\mathrm{K}$ and doping $\nu = -0.8$. The hue represents whether the spectral weight comes from the f_- (blue) or f_+ (orange) orbitals. Since this is on the hole-doped side of CNP, the occupation of the f_+ (orange) electrons is nearly zero. Dynamical correlations are unimportant in this sector and the energy of the corresponding spectral weight is set by the strain splitting. This spectral weight is precisely the content of the persistent feature, marked by the dashed horizontal line in Figs. 1(e)–1(g), and at this filling, is composed of f_+ (orange) electrons. The active sector is composed of the f_- (blue) electrons, whose occupation changes as a function of filling. This sector exhibits dynamical correlations, developing the Hubbard bands and the zero-bias resonance forming the cascades. At the considered filling, this spectral weight is pinned close to the Fermi level.

In agreement with the observations in the QTM experiment [16], this contribution is absent at the Γ_M point. We arrive at the conclusion that strain causes the flat bands to split (already as a single particle effect) into antibonding and bonding subsets, only one of which is active depending on whether the system is electron or hole doped. The inactive sector causes the filling-independent persistent feature, while the active sector is responsible for the correlations and cascade resets.

P-symmetry breaking and inverse compressibility. At very low T, symmetry-broken integer-filling insulators are more stable on the electron side [38,39]. Lattice relaxation effects are responsible for particle-hole symmetry breaking, as Hartree-Fock studies have shown [40,41]. Yet, mean-field solutions are unable to correctly capture the sawtooth behavior of compressibility and the negative compressibility regions [18,20,29,37].

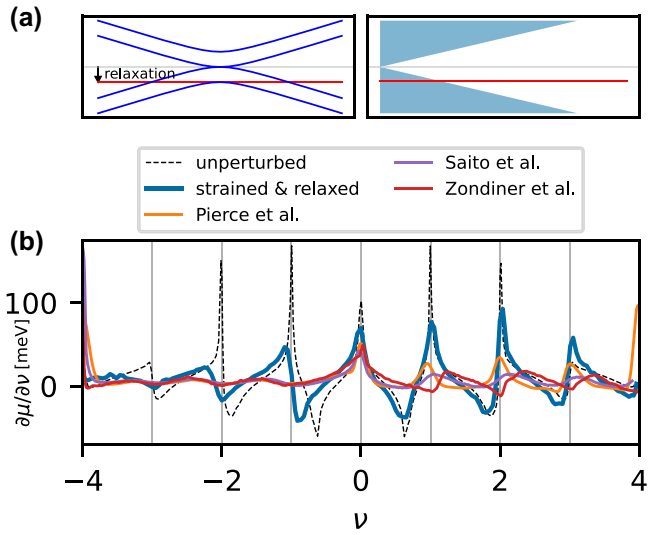


FIG. 3. (a) Sketch of the bare (zero-hybridization) dispersion of the f and c electrons in the relaxed THF model (left) and the corresponding density of states (right), (b) inverse charge compressibility $\partial\mu/\partial\nu$ as a function fo filling in TBLG with and without lattice relaxation and 0.15% strain and $T = 11.6$ K, compared with experimental data [18,20,37]. P-symmetry breaking due to lattice relaxation results in stronger peaks and troughs in the inverse compressibility on the electron-doped side.

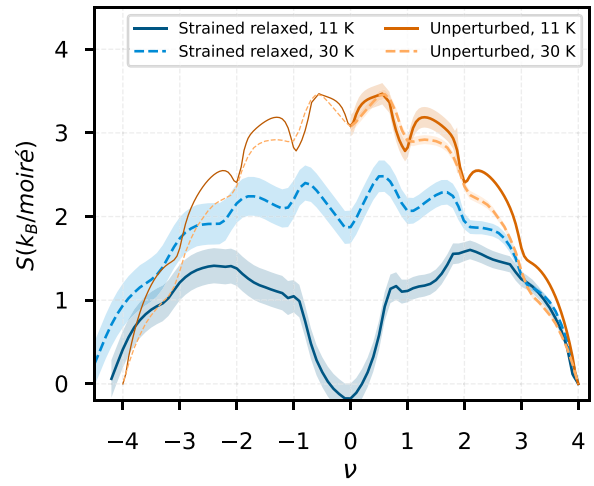


FIG. 4. Entropy as a function of filling of unperturbed TBLG (orange lines) compared to that of strained (0.15%) and relaxed TBLG (blue lines). The error bars (shaded area) are obtained by propagating the relative mean square deviation of a sample of DMFT-CTQMC iterations after convergence. In the unstrained case, the entropy on the hole-doping side is not calculated directly, since it is is determined by P symmetry. It is denoted by thin lines without error bars.

To explicitly quantify the impact of lattice relaxation induced P-symmetry breaking on theormodynamic observables, we study the relation between the chemical potential and the total filling. Figure 2(b) shows the inverse charge compressibility, $\partial\mu/\partial\nu$, of the strained and relaxed THF model compared to the unperturbed THF model from [29] and experimental data [18,20,37].

We find that the addition of strain and lattice relaxation terms allows us to capture an important qualitative feature missing in the unperturbed THF model. Multiple experiments [18,20,37] across different samples consistently find a strong particle-hole asymmetry: the variations in the charge compressibility are markedly stronger on the e-doped side compared to the h-doped side. The THF model with strain and lattice relaxation reproduces this phenomenon, and it can be understood by considering the primary effect of the lattice relaxation part of the Hamiltonian, which is a relative downward shift of the f-electron energies with respect to the charge neutrality point of the c Dirac bands. This is shown schematically in Fig. 3(a) where the bare f dispersion is represented by the red line, shifted down with respect to the touching point of the c bands. As a consequence, there is a higher c density of states available on the hole-doped side compared to the electron-doped side, and therefore there is stronger hybridization on the hole-doped side compared to the electron-doped side. This suppresses the local moment on the hole-doped side relative to the electron-doped side, which results in the softening of the compressibility variations. This is consistent with Hartree-Fock simulations which find that the ordered insulators on the electron-doped side have a larger gap than the ones on the hole-doped side [40,41]. Note that one might naively expect that since the upper flat band is more dispersive, correlations would be stronger on the hole-doped side. However, the crucial factor affecting the strength of correlations is the hybridization, which in turn correlates positively with the higher c density of states available on the hole-doped side.

Another key improvement with respect to previous simulations regards the position and shape of the inverse compressibility maxima. Though different experimental results show variations in the position and relative size of the peaks for electron doping (positive ν), the behavior for hole doping (negative ν) is remarkably consistent [17,18,20,37], and shows a marked depinning of the inverse compressibility maxima from integer total occupations. The inclusion of strain and relaxation terms immediately leads to a better estimation of the position and size of the compressibility maxima on the hole-doping side (blue solid line) with respect to the unstrained model [dashed black line in Fig. 3(b)]. The increased hybridization on the hole-doped side again plays a crucial role in the depinning. The hybridization has a smoothing effect making the f-sector less quantum-dot-like, lowering the penalty of noninteger occupation. In other words, the system is more metallic on the hole-doped side than on the electron-doped side (see further discussion in the Supplemental Material [25]).

Entropy. Entropy has been recently used to experimentally assess the presence and degeneracy of local moments in TBLG [5]. We calculate the entropy as a function of filling, for different values of temperature, by means of the Maxwell relation

$$S(\nu, T) = -\int_4^{\nu} \left(\frac{\partial\mu}{\partial T}\right)_{\nu'} d\nu', \tag{2}$$

where we assume that the band insulator at full filling ($\nu = 4$) has zero entropy.

Figure 4 shows the entropy of TBG with and without strain and relaxation at two temperatures. At 11 K, the

entropy curves with and without strain are qualitatively different. In the unstrained case, the entropy curve oscillates around a rough semicircular envelope spanning $\nu \in [-4, 4]$ with a maximum at the charge neutrality point. In contrast, in the strained case, the entropy goes to zero at the charge neutrality point, with two semicircular envelopes spanning $\nu \in [-4, 0]$ and $\nu \in [0, 4]$. This can be explained by the splitting of the eightfold degenerate flat-band manifold into two fourfold degenerate antibonding and bonding bands by strain. The vanishing entropy at the charge neutrality point is a consequence of the gap between the antibonding and bonding flat bands. At higher temperatures (30 K), thermal excitation can overcome the strain gap restoring the eightfold degeneracy of the local moments. The degeneracy is reflected in the fine features of the entropy curve. There are local maxima between neighboring integer fillings giving rise to an overall eight-lobed structure. Consequently, at high temperatures, both unstrained and strained data have the same qualitative features: eight lobes and finite entropy at CNP. The shape of the entropy curves match favorably with experimental measurements [5,17].

Discussion. The spectrosopic ± 10 meV feature, the evolution of entropy with filling and temperature, and the pronounced particle–hole asymmetry observed, for example, in charge compressibility measurements constitute key experimental constraints for a proper theoretical description of twisted bilayer graphene. Existing theoretical efforts have partially addressed this set of phenomena using a broad range of frameworks, including low-energy Dirac semimetals [17,20], interaction-induced band renormalizations [42,43], lifting of flavor degeneracies via spontaneous symmetry breaking or external perturbations [44,45], heavy-fermion and mixed-valence scenarios [5,46], incipient subband formation in paradigmatic Hubbard models [9,47], and exotic trion excitations [48,49]. However, a single microscopic framework capable of consistently accounting for all these effects has remained elusive.

Here, we showed that these seemingly distinct experimental signatures can only be understood by simultaneously accounting for correlations, strain, and lattice-relaxation effects inherent to realistic twisted bilayer graphene. We identified strain-induced splitting of the flat-band manifold as the central mechanism underlying both the emergence of a persistent feature in the local spectral density and the crossover from an eightfold-degenerate to a fourfold-degenerate local moment upon lowering the temperature [5]. At low temperatures, one of the two strain-split sectors becomes effectively inactive and is energetically positioned so as to account quantitatively for the persistent ± 10 meV feature observed in QTM and STM experiments. The freezing of this inactive sector naturally explains the reduction of the local-moment degeneracy, and our numerical estimates of the resulting entropy are in excellent agreement with recent experimental measurements.

The identification of an inactive charge sector also has important implications for future theoretical modeling of correlated states in twisted bilayer graphene [50]. Any faithful low-energy theory must incorporate the effective freezing of one sector upon lowering the temperature and collective instabilities—most prominently superconductivity—must be understood as arising within this constrained low-energy landscape. Finally, lattice relaxation and the associated breaking of particle-hole symmetry render the bonding flat bands more dispersive than the antibonding flat bands; this asymmetry is inherited by the interacting system and naturally leads to stronger correlation effects on the electron-doped side compared to the hole-doped side. More broadly, this work underscores the exceptional sensitivity of correlated quantum materials to externally imposed symmetry breaking, revealing a general route toward controlling collective electronic behavior.

Acknowledgments. We thank Oskar Vafek, Erez Berg, and Shahal Ilani for useful discussions. L.C., G.R., and T.W. acknowledge support from the Cluster of Excellence "CUI: Advanced Imaging of Matter" – EXC 2056 (Project No. 390715994), and SPP 2244 (WE 5342/5-1 Project No. 422707584). L.C. gratefully acknowledges the scientific support and HPC resources provided by the Erlangen National High Performance Computing Center (NHR@FAU) of the Friedrich-Alexander-Universität Erlangen-Nürnberg (FAU) under the NHR Project b158cb. G.R., L.C., R.V., G.S., and T.W. acknowledge support from the Deutsche Forschungsgemeinschaft (DFG, German Research Foundation) through QUAST FOR 5249 (Project No. 449872909 and Projects P4 and P5). G.S. acknowledges financial support by the Deutsche Forschungsgemeinschaft (DFG, German Research Foundation) under Germany's Excellence Strategy–EXC2147 "ctd.qmat" (Project ID 390858490). R.V. thanks the Deutsche Forschungsgemeinschaft (DFG, German Research Foundation) through the TRR 288 - 422213477 and Project No. VA 117/23-1 — 509751747. B.A.B. and H.H. were supported by the Gordon and Betty Moore Foundation through Grant No. GBMF8685 toward the Princeton theory program, the Gordon and Betty Moore Foundation's EPiQS Initiative (Grant No. GBMF11070), the Office of Naval Research (ONR Grant No. N00014-20-1-2303), the Global Collaborative Network Grant at Princeton University, the Simons Investigator Grant - MPS-SIP-00404513, the NSF MRSEC - DMR 2011750, the Simons Collaboration on New Frontiers in Superconductivity (SFI-MPS- NFS-00006741-01), the Schmidt Foundation at Princeton University, and the Princeton Catalyst Initiative. H.H. and D.C. also acknowledge support from the European Research Council (ERC) under the European Union's Horizon 2020 research and innovation program (Grant Agreement No. 101020833).

Data availability. The data that support the findings of this article are openly available at [51]

[1] K. P. Nuckolls, R. L. Lee, M. Oh, D. Wong, T. Soejima, J. P. Hong, D. Călugăru, J. Herzog-Arbeitman, B. A. Bernevig, K. Watanabe, T. Taniguchi, N. Regnault, M. P. Zaletel, and A. Yazdani, Quantum textures of the many-body wavefunctions in magic-angle graphene, Nature (London) **620**, 525 (2023).

[2] A. Kerelsky, L. J. McGilly, D. M. Kennes, L. Xian, M. Yankowitz, S. Chen, K. Watanabe, T. Taniguchi, J. Hone, C. Dean, A. Rubio, and A. N. Pasupathy, Maximized electron interactions at the magic angle in twisted bilayer graphene, Nature (London) **572**, 95 (2019).

[3] S. Turkel, J. Swann, Z. Zhu, M. Christos, K. Watanabe, T. Taniguchi, S. Sachdev, M. S. Scheurer, E. Kaxiras, C. R. Dean, and A. N. Pasupathy, Orderly disorder in magic-angle twisted trilayer graphene, Science **376**, 193 (2022).

[4] N. P. Kazmierczak, M. Van Winkle, C. Ophus, K. C. Bustillo, S. Carr, H. G. Brown, J. Ciston, T. Taniguchi, K. Watanabe, and D. K. Bediako, Strain fields in twisted bilayer graphene, Nat. Mater. **20**, 956 (2021).

[5] Z. Zhang, S. Wu, D. Călugăru, H. Hu, T. Taniguchi, K. Wanatabe, A. B. Bernevig, and E. Y. Andrei, Heavy fermions, mass renormalization and local moments in magic-angle twisted bilayer graphene via planar tunneling spectroscopy, arXiv:2503.17875.

[6] Y. Cao, V. Fatemi, A. Demir, S. Fang, S. L. Tomarken, J. Y. Luo, J. D. Sanchez-Yamagishi, K. Watanabe, T. Taniguchi, E. Kaxiras, R. C. Ashoori, and P. Jarillo-Herrero, Correlated insulator behaviour at half-filling in magic-angle graphene superlattices, Nature (London) **556**, 80 (2018).

[7] K. P. Nuckolls, M. Oh, D. Wong, B. Lian, K. Watanabe, T. Taniguchi, B. A. Bernevig, and A. Yazdani, Strongly correlated Chern insulators in magic-angle twisted bilayer graphene, Nature (London) **588**, 610 (2020).

[8] P. Stepanov, M. Xie, T. Taniguchi, K. Watanabe, X. Lu, A. H. MacDonald, B. A. Bernevig, and D. K. Efetov, Competing zero-field Chern insulators in superconducting twisted bilayer graphene, Phys. Rev. Lett. **127**, 197701 (2021).

[9] D. Wong, K. P. Nuckolls, M. Oh, B. Lian, Y. Xie, S. Jeon, K. Watanabe, T. Taniguchi, B. A. Bernevig, and A. Yazdani, Cascade of electronic transitions in magic-angle twisted bilayer graphene, Nature (London) **582**, 198 (2020).

[10] Y. Xie, B. Lian, B. Jäck, X. Liu, C.-L. Chiu, K. Watanabe, T. Taniguchi, B. A. Bernevig, and A. Yazdani, Spectroscopic signatures of many-body correlations in magic-angle twisted bilayer graphene, Nature (London) **572**, 101 (2019).

[11] Y. Choi, J. Kemmer, Y. Peng, A. Thomson, H. Arora, R. Polski, Y. Zhang, H. Ren, J. Alicea, G. Refael, F. von Oppen, K. Watanabe, T. Taniguchi, and S. Nadj-Perge, Electronic correlations in twisted bilayer graphene near the magic angle, Nat. Phys. **15**, 1174 (2019).

[12] Z. Hao, A. M. Zimmerman, P. Ledwith, E. Khalaf, D. H. Najafabadi, K. Watanabe, T. Taniguchi, A. Vishwanath, and P. Kim, Electric field–tunable superconductivity in alternating-twist magic-angle trilayer graphene, Science **371**, 1133 (2021).

[13] J. Yu, B. A. Foutty, Y. H. Kwan, M. E. Barber, K. Watanabe, T. Taniguchi, Z.-X. Shen, S. A. Parameswaran, and B. E. Feldman, Spin skyrmion gaps as signatures of strong-coupling insulators in magic-angle twisted bilayer graphene, Nat. Commun. **14**, 6679 (2023).

[14] R. Bistritzer and A. H. MacDonald, Moiré bands in twisted double-layer graphene, Proc. Natl. Acad. Sci. USA **108**, 12233 (2011).

[15] J. Herzog-Arbeitman, J. Yu, D. Calugaru, H. Hu, N. Regnault, O. Vafek, J. Kang, and B. A. Bernevig, Topological heavy fermion model as an efficient representation of atomistic strain and relaxation in twisted bilayer graphene, Phys. Rev. B **112**, 125128 (2025).

[16] J. Xiao, A. Inbar, J. Birkbeck, N. Gershon, Y. Zamir, Y. Vituri, T. Taniguchi, K. Watanabe, E. Berg, and S. Ilani, Imaging the flat bands of magic-angle graphene reshaped by interactions, Nature (London) **653**, 68 (2026).

[17] A. Rozen, J. M. Park, U. Zondiner, Y. Cao, D. Rodan-Legrain, T. Taniguchi, K. Watanabe, Y. Oreg, A. Stern, E. Berg, P. Jarillo-Herrero, and S. Ilani, Entropic evidence for a Pomeranchuk effect in magic-angle graphene, Nature (London) **592**, 214 (2021).

[18] Y. Saito, F. Yang, J. Ge, X. Liu, T. Taniguchi, K. Watanabe, J. I. A. Li, E. Berg, and A. F. Young, Isospin Pomeranchuk effect in twisted bilayer graphene, Nature (London) **592**, 220 (2021).

[19] I. Das, X. Lu, J. Herzog-Arbeitman, Z.-D. Song, K. Watanabe, T. Taniguchi, B. A. Bernevig, and D. K. Efetov, Symmetry-broken Chern insulators and Rashba-like Landau-level crossings in magic-angle bilayer graphene, Nat. Phys. **17**, 710 (2021).

[20] A. T. Pierce, Y. Xie, J. M. Park, E. Khalaf, S. H. Lee, Y. Cao, D. E. Parker, P. R. Forrester, S. Chen, K. Watanabe, T. Taniguchi, A. Vishwanath, P. Jarillo-Herrero, and A. Yacoby, Unconventional sequence of correlated Chern insulators in magic-angle twisted bilayer graphene, Nat. Phys. **17**, 1210 (2021).

[21] Y. Cao, V. Fatemi, S. Fang, K. Watanabe, T. Taniguchi, E. Kaxiras, and P. Jarillo-Herrero, Unconventional superconductivity in magic-angle graphene superlattices, Nature (London) **556**, 43 (2018).

[22] X. Lu, P. Stepanov, W. Yang, M. Xie, M. A. Aamir, I. Das, C. Urgell, K. Watanabe, T. Taniguchi, G. Zhang, A. Bachtold, A. H. MacDonald, and D. K. Efetov, Superconductors, orbital magnets and correlated states in magic-angle bilayer graphene, Nature (London) **574**, 653 (2019).

[23] M. Yankowitz, S. Chen, H. Polshyn, Y. Zhang, K. Watanabe, T. Taniguchi, D. Graf, A. F. Young, and C. R. Dean, Tuning superconductivity in twisted bilayer graphene, Science **363**, 1059 (2019).

[24] Z.-D. Song and B. A. Bernevig, Magic-angle twisted bilayer graphene as a topological heavy fermion problem, Phys. Rev. Lett. **129**, 047601 (2022).

[25] See Supplemental Material at http://link.aps.org/supplemental/10.1103/x2mz-hm8y for additional information on the model, solution method, and interplay between strain and level splitting, which includes Refs. [52–56].

[26] S. Carr, D. Massatt, S. B. Torrisi, P. Cazeaux, M. Luskin, and E. Kaxiras, Relaxation and domain formation in incommensurate two-dimensional heterostructures, Phys. Rev. B **98**, 224102 (2018).

[27] O. Vafek and J. Kang, Continuum effective Hamiltonian for graphene bilayers for an arbitrary smooth lattice deformation from microscopic theories, Phys. Rev. B **107**, 075123 (2023).

[28] J. Kang and O. Vafek, Analytical solution for the relaxed atomic configuration of twisted bilayer graphene including heterostrain, Phys. Rev. B **112**, 125138 (2025).

[29] G. Rai, L. Crippa, D. Călugăru, H. Hu, F. Paoletti, L. de' Medici, A. Georges, B. A. Bernevig, R. Valentí,

G. Sangiovanni, and T. Wehling, Dynamical correlations and order in magic-angle twisted bilayer graphene, Phys. Rev. X **14**, 031045 (2024).

[30] A. Datta, M. J. Calderón, A. Camjayi, and E. Bascones, Heavy quasiparticles and cascades without symmetry breaking in twisted bilayer graphene, Nat. Commun. **14**, 5036 (2023).

[31] H. Hu, G. Rai, L. Crippa, J. Herzog-Arbeitman, D. Călugăru, T. Wehling, G. Sangiovanni, R. Valentí, A. M. Tsvelik, and B. A. Bernevig, Symmetric Kondo lattice states in doped strained twisted bilayer graphene, Phys. Rev. Lett. **131**, 166501 (2023).

[32] M. Wallerberger, A. Hausoel, P. Gunacker, A. Kowalski, N. Parragh, F. Goth, K. Held, and G. Sangiovanni, W2dynamics: Local one- and two-particle quantities from dynamical mean field theory, Comput. Phys. Commun. **235**, 388 (2019).

[33] H. Kim, Y. Choi, É. Lantagne-Hurtubise, C. Lewandowski, A. Thomson, L. Kong, H. Zhou, E. Baum, Y. Zhang, L. Holleis, K. Watanabe, T. Taniguchi, A. F. Young, J. Alicea, and S. Nadj-Perge, Imaging inter-valley coherent order in magic-angle twisted trilayer graphene, Nature (London) **623**, 942 (2023).

[34] X.-F. Zhou, Y.-W. Liu, C.-Y. Hao, C. Yan, Q. Zheng, Y.-N. Ren, Y.-X. Zhao, K. Watanabe, T. Taniguchi, and L. He, Coexistence of reconstructed and unreconstructed structures in the structural transition regime of twisted bilayer graphene, Phys. Rev. B **107**, 125410 (2023).

[35] A. Inbar, J. Birkbeck, J. Xiao, T. Taniguchi, K. Watanabe, B. Yan, Y. Oreg, A. Stern, E. Berg, and S. Ilani, The quantum twisting microscope, Nature (London) **614**, 682 (2023).

[36] M. Lee, I. Das, J. Herzog-Arbeitman, J. Papp, J. Li, M. Daschner, Z. Zhou, M. Bhatt, M. Currle, J. Yu, Y. Jiang, M. Becherer, R. Mittermeier, P. Altpeter, C. Obermayer, H. Lorenz, G. Chavez, B. T. Le, J. Williams, K. Watanabe, *et al.*, Revealing electron-electron interactions in graphene at room temperature with the quantum twisting microscope, Nano Lett. **26**, 4046 (2026).

[37] U. Zondiner, A. Rozen, D. Rodan-Legrain, Y. Cao, R. Queiroz, T. Taniguchi, K. Watanabe, Y. Oreg, F. von Oppen, A. Stern, E. Berg, P. Jarillo-Herrero, and S. Ilani, Cascade of phase transitions and Dirac revivals in magic-angle graphene, Nature (London) **582**, 203 (2020).

[38] P. Stepanov, I. Das, X. Lu, A. Fahimniya, K. Watanabe, T. Taniguchi, F. H. L. Koppens, J. Lischner, L. Levitov, and D. K. Efetov, Untying the insulating and superconducting orders in magic-angle graphene, Nature (London) **583**, 375 (2020).

[39] Y. Saito, J. Ge, K. Watanabe, T. Taniguchi, and A. F. Young, Independent superconductors and correlated insulators in twisted bilayer graphene, Nat. Phys. **16**, 926 (2020).

[40] Y. H. Kwan, G. Wagner, T. Soejima, M. P. Zaletel, S. H. Simon, S. A. Parameswaran, and N. Bultinck, Kekulé spiral order at all nonzero integer fillings in twisted bilayer graphene, Phys. Rev. X **11**, 041063 (2021).

[41] G. Wagner, Y. H. Kwan, N. Bultinck, S. H. Simon, and S. A. Parameswaran, Global phase diagram of the normal state of twisted bilayer graphene, Phys. Rev. Lett. **128**, 156401 (2022).

[42] L. Rademaker, D. A. Abanin, and P. Mellado, Charge smoothening and band flattening due to Hartree corrections in twisted bilayer graphene, Phys. Rev. B **100**, 205114 (2019).

[43] J. Zhu, I. Torre, M. Polini, and A. H. MacDonald, Weak-coupling theory of magic-angle twisted bilayer graphene, Phys. Rev. B **110**, L121117 (2024).

[44] M. Xie and A. H. MacDonald, Weak-field Hall resistivity and spin-valley flavor symmetry breaking in magic-angle twisted bilayer graphene, Phys. Rev. Lett. **127**, 196401 (2021).

[45] N. Bultinck, E. Khalaf, S. Liu, S. Chatterjee, A. Vishwanath, and M. P. Zaletel, Ground state and hidden symmetry of magic-angle graphene at even integer filling, Phys. Rev. X **10**, 031034 (2020).

[46] L. L. H. Lau and P. Coleman, Topological mixed valence model for twisted bilayer graphene, Phys. Rev. X **15**, 021028 (2025).

[47] A. Ghosh, S. Chakraborty, R. Dutta, A. Agarwala, K. Watanabe, T. Taniguchi, S. Banerjee, N. Trivedi, S. Mukerjee, and A. Das, Thermopower probes of emergent local moments in magic-angle twisted bilayer graphene, Nat. Phys. **21**, 732 (2025).

[48] J.-Y. Zhao, B. Zhou, and Y.-H. Zhang, Topological Mott localization and pseudogap metal in twisted bilayer graphene, Phys. Rev. B **112**, 085107 (2025).

[49] P. J. Ledwith, J. Dong, A. Vishwanath, and E. Khalaf, Nonlocal moments in the Chern bands of twisted bilayer graphene, Phys. Rev. X **15**, 021087 (2025).

[50] G.-D. Zhou, Y.-J. Wang, N. Tong, and Z.-D. Song, Kondo phase in twisted bilayer graphene, Phys. Rev. B **109**, 045419 (2024).

[51] L. Crippa, Figure data for interplay between many-body correlations, strain and lattice relaxation in twisted bilayer graphene [Data set], Zenodo (2026), https://doi.org/10.5281/zenodo.20427082.

[52] J. Kaufmann and K. Held, ana_cont: Python package for analytic continuation, Comput. Phys. Commun. **282**, 108519 (2023).

[53] N. Wagner, L. Crippa, A. Amaricci, P. Hansmann, M. Klett, E. J. König, T. Schäfer, D. D. Sante, J. Cano, A. J. Millis, A. Georges, and G. Sangiovanni, Mott insulators with boundary zeros, Nat. Commun. **14**, 7531 (2023).

[54] H. Shinaoka, Y. Nomura, S. Biermann, M. Troyer, and P. Werner, Negative sign problem in continuous-time quantum Monte Carlo: Optimal choice of single-particle basis for impurity problems, Phys. Rev. B **92**, 195126 (2015).

[55] A. Georges, G. Kotliar, W. Krauth, and M. J. Rozenberg, Dynamical mean-field theory of strongly correlated fermion systems and the limit of infinite dimensions, Rev. Mod. Phys. **68**, 13 (1996).

[56] E. Gull, A. J. Millis, A. I. Lichtenstein, A. N. Rubtsov, M. Troyer, and P. Werner, Continuous-time Monte Carlo methods for quantum impurity models, Rev. Mod. Phys. **83**, 349 (2011).